



OPEN ACCESS

**Edited by:**

Giuseppe Piscosquito,  
Fondazione Salvatore Maugeri  
(IRCCS), Italy

**Reviewed by:**

Fiore Manganelli,  
University of Naples Federico II, Italy  
Dies Meijer,  
University of Edinburgh,  
United Kingdom

**\*Correspondence:**

Lucilla Nobbio  
lnobbio@neurologia.unige.it

† These authors have contributed  
equally to this work

**‡ Present address:**

Abdul Basit,  
Department of Pharmaceuticals,  
University of Washington, Seattle, WA,  
United States  
Adrienne M. Luoma,  
Department of Cancer Immunology  
and Virology, Dana-Farber Cancer  
Institute; Department of Microbiology  
and Immunobiology, Harvard Medical  
School, Boston, MA, United States

**Specialty section:**

This article was submitted to  
Neuromuscular Diseases,  
a section of the journal  
Frontiers in Neurology

**Received:** 12 February 2020

**Accepted:** 14 July 2020

**Published:** 25 August 2020

**Citation:**

Visigalli D, Capodivento G, Basit A,  
Fernández R, Hamid Z, Pencová B,  
Gemelli C, Marubbi D, Pastorino C,  
Luoma AM, Riekel C, Kirschner DA,  
Schenone A, Fernández JA,  
Armirotti A and Nobbio L (2020)  
Exploiting Sphingo- and  
Glycerophospholipid Impairment to  
Select Effective Drugs and Biomarkers  
for CMT1A. *Front. Neurol.* 11:903.  
doi: 10.3389/fneur.2020.00903

# Exploiting Sphingo- and Glycerophospholipid Impairment to Select Effective Drugs and Biomarkers for CMT1A

**Davide Visigalli<sup>1,2†</sup>, Giovanna Capodivento<sup>1,2†</sup>, Abdul Basit<sup>3‡</sup>, Roberto Fernández<sup>4</sup>, Zeeshan Hamid<sup>3</sup>, Barbora Pencová<sup>4</sup>, Chiara Gemelli<sup>1,2</sup>, Daniela Marubbi<sup>5,6</sup>, Cecilia Pastorino<sup>1,2</sup>, Adrienne M. Luoma<sup>7‡</sup>, Christian Riekel<sup>8</sup>, Daniel A. Kirschner<sup>7</sup>, Angelo Schenone<sup>1,2</sup>, José A. Fernández<sup>4</sup>, Andrea Armirotti<sup>3</sup> and Lucilla Nobbio<sup>1,2\*</sup>**

<sup>1</sup> DINOGLMI, University of Genoa, Genoa, Italy, <sup>2</sup> IRCCS Ospedale Policlinico S. Martino, UO Clinica Neurologica, Genoa, Italy, <sup>3</sup> Analytical Chemistry Lab, Fondazione Istituto Italiano di Tecnologia, Genoa, Italy, <sup>4</sup> Department of Physical Chemistry, Faculty of Science and Technology, University of the Basque Country, Leioa, Spain, <sup>5</sup> DIMES, University of Genoa, Genoa, Italy, <sup>6</sup> IRCCS Ospedale Policlinico S. Martino, UO Oncologia Cellulare Genoa, Genoa, Italy, <sup>7</sup> Department of Biology, Boston College, Boston, MA, United States, <sup>8</sup> The European Synchrotron, ESRF, Grenoble, France

In Charcot–Marie–Tooth type 1A (CMT1A), Schwann cells exhibit a preponderant transcriptional deficiency of genes involved in lipid biosynthesis. This perturbed lipid metabolism affects the peripheral nerve physiology and the structure of peripheral myelin. Nevertheless, the identification and functional characterization of the lipid species mainly responsible for CMT1A myelin impairment currently lack. This is critical in the pathogenesis of the neuropathy since lipids are many and complex molecules which play essential roles in the cell, including the structural components of cellular membranes, cell signaling, and membrane trafficking. Moreover, lipids themselves are able to modify gene transcription, thereby affecting the genotype–phenotype correlation of well-defined inherited diseases, including CMT1A. Here we report for the first time a comprehensive lipid profiling in experimental and human CMT1A, demonstrating a previously unknown specific alteration of sphingolipid (SP) and glycerophospholipid (GP) metabolism. Notably, SP, and GP changes even emerge in biological fluids of CMT1A rat and human patients, implying a systemic metabolic dysfunction for these specific lipid classes. Actually, SP and GP are not merely reduced; their expression is instead aberrant, contributing to the ultrastructural abnormalities that we detailed by X-ray diffraction in rat and human internode myelin. The modulation of SP and GP pathways in myelinating dorsal root ganglia cultures clearly sustains this issue. In fact, just selected molecules interacting with these pathways are able to modify the altered geometric parameters of CMT1A myelinated fibers. Overall, we propose to exploit the present SP and GP metabolism impairment to select effective drugs and validate a set of reliable biomarkers, which remain a challenge in CMT1A neuropathy.

**Keywords:** CMT1A, biomarker, drug, myelin, lipid metabolism, Schwann cell, demyelination, peripheral neuropathy

## INTRODUCTION

Charcot–Marie–Tooth (CMT) neuropathies are a group of inherited diseases affecting peripheral nerve function. Among them, CMT type 1A (CMT1A) is the most prevalent type, displaying characteristic dys/demyelination that still rules its own classification (1, 2). The genetic defect responsible for CMT1A, a 1.5-Mb duplication on chromosome 17p11.2 containing the *PMP22* gene, was identified more than 20 years ago (3–6); however, this revelation has not led to the ultimate comprehension of CMT1A genotype–phenotype correlation yet nor to an effective therapy (7, 8). In fact, CMT1A patients sharing the same genetic defect experience a remarkable phenotypic diversity and severity (9–11).

As for other hereditary neuromuscular diseases in which gene therapy proved to be effective, the negative regulation of *PMP22* expression represents the ideal biological endpoint and therapeutic goal (12–14). To date, in contrast to preclinical studies, clinical trials in CMT1A patients aimed to down-regulate *PMP22* showed negative results (7, 15–17). Furthermore, gene therapy, in addition to the obvious technical difficulties, seems to be still poorly acceptable for CMT1A patients in which life expectancy and quality of life are not dramatically affected (18, 19). Alternative therapeutic options should be explored, as previously suggested (20–25).

In this context, we focused on dys/demyelination as a critical target downstream of the *PMP22* defect, assuming that the refined knowledge of lipid metabolism is essential to effectively address this aspect (26).

Indeed myelin chemical composition, structure, and physiology are intimately related and altered in several dysmyelinating neuropathies, including CMT1A (27–32). Moreover, peripheral myelin distress is caused by mutations in a variety of genes, including those coding for enzymes involved in lipid biosynthesis and metabolism (33–37). Notably, several molecules modulate the activity of these enzymes and are used as real drugs in pathological conditions (38). Recent studies demonstrated that soy phospholipid and high-fat neutral lipid-enriched diets improve myelination in CMT1A and CMT1E animal models (30, 39). It has also been shown that changes in the circulating lipid profile may be related to the onset, activity, and progression of some important human diseases, including myelin disorders (40–42).

In spite of these observations, lipid metabolism still remains largely under-explored in CMT neuropathies, including CMT1A (39). In fact, it is vital to identify and characterize lipid species and their changes, biological role, and mutual interaction (43).

In the present study, we addressed this gap by a multi-disciplinary and technologically advanced approach, performing a comprehensive study of lipid metabolism both in experimental and in human CMT1A.

We found that sphingolipid and glycerophospholipid (SP and GP) pathways are mainly responsible for the perturbed lipid metabolism already described in CMT1A (30). We also found a systemic alteration of SP and GP metabolism in experimental and in human CMT1A biological fluids. Notably, the specific targeting of just these pathways was able to

improve the altered structural parameters of CMT1A myelinated fibers *in vitro*.

## MATERIALS AND METHODS

### Animal Model

The CMT rat, an animal model of CMT1A neuropathy originally developed in K-A Nave laboratory, was used for the experiments (44). Sixty-day-old heterozygous CMT1A animals and wild-type (WT) littermates of both sexes were used for most of the experiments unless otherwise specified. We confirm that all methods were performed in accordance with relevant guidelines/regulations. In particular, the research protocols presented in this study are conducted in accordance with the ARRIVE guidelines and are included in those reviewed and approved by the OPBA (Institutional Animal Welfare Body) and by the Italian Ministry of Health (project number approval 798/2016-PR).

### Cell Culture and Drug Administration

Myelinating dorsal root ganglia (DRG) cultures were established from 15-day-old embryos as previously described (29, 45–47). Briefly, 35–40 DRG were removed from each embryo, incubated for 30 min with 0.25% trypsin in Hanks' solution, and minced to obtain a suspension of DRG cells. The cells were washed and dissolved in complete medium made up of neurobasal medium (Invitrogen) supplemented with 15% newborn calf serum, ascorbic acid (100 µg/ml), and nerve growth factor at 5 ng/ml. This suspension was plated on collagen-coated ACLAR dishes at a density of  $15 \times 10^4$  cells/dish.

Both CMT1A and WT DRG cultures were grown in complete medium and chronically treated with different molecules interfering with SP and GP metabolism (see also **Figure 3A**). In particular, the cultures were treated every other day for 30 days with oleyl-L- $\alpha$ -lysophosphatidic acid (LPA) (Na<sup>+</sup> salt) (Sigma-Aldrich, L7260), L- $\alpha$ -phosphatidic acid (PA) (Na<sup>+</sup> salt) (Sigma-Aldrich, P9511), CDP-choline (Na<sup>+</sup> salt) (Sigma-Aldrich, C0256), VO-OHpic trihydrate (a PTEN inhibitor) (Sigma-Aldrich, V8639), phosphatidylinositol tris-3,4,5-phosphate (Na<sup>+</sup> salt) (PIP3) (Matreya, Restek Superchrom, 1775-1), desipramine hydrochloride (Sigma-Aldrich, D3900), sphingomyelin (Sigma-Aldrich, S0074), L-serine (Sigma-Aldrich, S4311), and 2-hydroxy oleic acid (2OHOA) (Sigma-Aldrich, SML0256). The vehicle was represented by distilled water (ddH<sub>2</sub>O) for L-serine, PIP3, desipramine, and CDP-choline, Dulbecco's phosphate-buffered saline (DPBS) (Gibco, 14190-144) for LPA, PA, and dimethyl sulfoxide (Sigma, D8418) for VO-OHpic, and 2OHOA and absolute ethanol for sphingomyelin, respectively. At the end of each treatment, the DRG cultures were processed for advanced quantitative neuropathology (see below).

Preliminary dose–response experiments were performed for each molecule, including the vehicle to define safety and effectiveness (data available at request). The sample size of the treatment groups was calculated with PASS 11 (<http://www.ncss.com/software/pass/>). The power analysis was performed in *a priori* manner. Type I error was given with 5% and type II error was given with  $\geq 90\%$ . Myelin density and internode

length served as main outcome measures for the power analysis. Assuming a complete recovery of the phenotype as the endpoint, mean post-treatment differences of  $5 \times 10^{-5}$  units for myelin density and of 13.67 units for internode length are required for the CMT1A DRG cultures. We calculated a sample size of three cultures for each group to reach a statistical power higher than 90% (97 and 98%, respectively). The most effective dosage for the molecules displaying a significant effect on the geometric parameters of myelinated fibers was validated on a second round of experiments. In particular, we analyzed the effect of LPA (0.1  $\mu$ M), PIP3 (2  $\mu$ M), L-serine (0.5 mM), and VO-OHpic (0.1  $\mu$ M) on CMT1A and WT DRG cultures.

## Samples From Human Subjects

The subjects involved in this exploratory study included 15 healthy controls (eight females and seven males, mean age:  $47 \pm 11$  years, range: 27–67 years) and 28 patients with clinical and genetic diagnosis of CMT1A (18 females and 10 males, mean age:  $55 \pm 15$  years, range: 22–82 years). Our small cohort of patients displayed a mean CMTNS of  $13.35 \pm 5.78$  (95% CI, 10.64–16.06) in agreement with the most frequent phenotype observed in CMT1A populations (48). We confirm that all methods were performed in accordance with relevant guidelines/regulations. The Regional Ethics Committee (CER Liguria) approved the current study protocol (project number approval 545REG2015), and the patients gave written informed consent according to the Helsinki Declaration as revised in 2013. Peripheral blood (5 ml) from CMT1A patients and controls was added to collection tubes containing a clot activator and spun to obtain the serum fraction. Serum was immediately frozen and stored at  $-80^\circ\text{C}$  in 500- $\mu$ l aliquots to perform lipidomics; repeated freezing and thawing was avoided. The archived sural nerve biopsies from patients with CMT1A and from subjects who underwent nerve biopsy for suspected peripheral neuropathy were also used to perform X-ray diffraction analysis.

## Isolation of PNS Myelin

Rat sciatic nerves were used to prepare myelin-enriched fraction as previously described (32, 49).

## Rat CSF and Serum Collection

Cerebrospinal fluid (CSF) collection was performed according to Liu et al. (50). Briefly, the rats were anesthetized with an intraperitoneal injection of ketamine/xylazine cocktail (100:10 mg/kg) and tightly fixed on ear bars to immobilize the head of the animals. The skin at the base of the neck was removed and the CSF was collected through a cisterna magna puncture technique, and immediately frozen at  $-80^\circ\text{C}$ . Serum collection was performed from the retro-orbital plexus by a capillary tube. The blood was clotted at room temperature and centrifuged prior to freezing the serum at  $-80^\circ\text{C}$ . All the procedures were performed according to the ARRIVE guidelines.

## Lipidomics by LC-MS/MS

Lipids were extracted from sciatic nerves, purified myelin, and biological fluids by using the Bligh–Dyer protocol (51). In brief, 2 ml of 1:2 chloroform/methanol mixture (v/v) was added to

the vials and vortexed for 30 s. Chloroform (0.5 ml) and water (0.5 ml) were then sequentially added and thoroughly mixed after each addition. The samples were then centrifuged for 15 min at  $3,500 \times g$  at room temperature (RT). At the end of the process, the organic (lower) phase ( $\sim 1.5$  ml) was transferred to glass vials. The aqueous phases were re-extracted to increase the overall recovery. The organic phases from both extractions were pooled in a glass vial and dried under a nitrogen stream. The extracted lipids were re-dissolved in 0.1 ml of a 9:1 methanol/chloroform solution and analyzed by liquid chromatography coupled to high-resolution mass spectrometry (MS).

Untargeted lipidomics of lipid extracts was performed on a UPLC Acquity system coupled to a Synapt G2 QToF high-resolution mass spectrometer. The lipids were separated on a CSH C18 column (1.7 M particle size,  $2.1 \times 100$  mm). Mobile phase A consisted of acetonitrile/water (60:40) with 10 mM ammonium formate, and mobile phase B consisted of acetonitrile/isopropyl alcohol (10:90) with 10 mM ammonium formate. The following gradient program was applied: 15% B for 1 min after injection, then increased to 60% B in 9 min, then to 75% B in 8 min, and then to 100% B for a further 2.5 min. An isocratic 100% B step was then maintained for 2.5 min, and the column was subsequently reconditioned to 15% B for 2 min. Total run time was 25 min with the following conditions: flow rate—0.4 ml/min, column temperature— $55^\circ\text{C}$ , and injection volume—6  $\mu$ l. The instrument was operated in positive electrospray ionization (ESI) mode. The MS source parameters were as follows: capillary and cone voltages were set at 2.8 kV and 30 V, respectively, source and desolvation temperature were set at 100 and  $450^\circ\text{C}$ , respectively, and desolvation gas and cone gas ( $\text{N}_2$ ) flows were set at 800 and 50 L/h, respectively. The mass spectra were recorded in MSe mode, with MS/MS fragmentation performed in the trap region on the instrument. Low-energy scans were acquired at a fixed 4 eV collision energy, and high-energy scans were acquired using a collision energy ramp from 20 to 40 eV. The spectra were recorded at a mass resolution of 20,000 in the range of 50–1,200 m/z. The scan rate was set to 0.3 spectra per second. A leucine-enkephalin solution (2 ng/ml) was continuously infused in the ESI source (4  $\mu$ l/min) and acquired every 30 s for real-time mass axis recalibration (52). All the samples were run in random order. Quality control samples, consisting of a pool of all the samples, were acquired and were used to assess system suitability, performance, and reproducibility.

## LC-MS/MS Data Analysis

Raw data were analyzed using MarkerLynx software (Waters Inc.) to re-align the observed peak and extract all the relevant features (53). The feature list was then analyzed with MetaboAnalyst 4.0, a web-based metabolomic data processing tool (54). Following principal component analysis (PCA), heatmap analyses were performed to detect the features showing significant changes between the groups. Lipid identification was then performed by interrogating the web-based algorithm HMDB using the accurate mass measured for each feature. The following adduct species were searched:  $[\text{M} + \text{H}]^+$ ,  $[\text{M} + \text{NH}_4]^+$ ,  $[\text{M} + \text{H}-\text{H}_2\text{O}]^+$ ,  $[\text{M} + \text{Na}]^+$ ,  $[\text{M} + \text{H}-2\text{H}_2\text{O}]^+$ ,  $[\text{M}$

+ CH<sub>3</sub>CN + H)<sup>+</sup>, [M + NH<sub>4</sub>-H<sub>2</sub>O]<sup>+</sup>, [M + isopropanol + Na]<sup>+</sup>, [M + 2CH<sub>3</sub>CN + H]<sup>+</sup>, [M + 2Na-H]<sup>+</sup>, and [M + K]<sup>+</sup>. A maximum of 5 ppm tolerance in mass accuracy was allowed. Whenever possible, feature annotation was also supported by tandem mass data (MSe mode) and class-specific retention time (55). Based on the putative ID of the statistically relevant features, pathway analysis was performed using a hypergeometric test for overrepresentation and using a *Rattus norvegicus* or *Homo sapiens* metabolite background.

## X-ray Diffraction Analysis

### Rat Sciatic Nerve

The fixed dissected sciatic nerves, prepared from rats that were 1.5 and 3 months old, were tied off at their ends and sealed, in contact with excess buffered fixative, in 0.7-mm-diameter quartz capillary tubes. X-ray diffraction spectra were recorded from the nerves using nickel-filtered, single-mirror-focused CuK $\alpha$  radiation from a fine-line source on a 3.0-kW Rigaku X-ray generator that was outfitted with a linear, position-sensitive detector, as described in Avila et al. (56). The myelin periodicity was calculated from the positions of the Bragg reflections in the patterns. The relative amount of multilamellar myelin was determined by measuring the total integrated intensity of the Bragg reflections ( $M$ ) above background ( $B$ ). The fraction of scattered intensity that is due to myelin is then  $M/(M + B)$  (56).

### Human Sural Nerve Biopsy

Small-angle X-ray scattering (SAXS) experiments were performed at the ID13 beamline of the European Synchrotron Radiation Facility (ESRF). The pink beam from an undulator was monochromated to a wavelength of  $\lambda = 0.09755$  nm, with  $\Delta\lambda/\lambda \sim 2 \times 10^{-4}$  by a liquid-N<sub>2</sub>-cooled Si crystal. Epon-embedded longitudinal and transversal sections of control human and CMT1A sural nerve samples were deposited on plain mesh TEM grids (57). A protein crystallography microgoniometer with on-axis optical microscopy allowed obtaining SAXS patterns at specific locations and extracting bilayer periods from the observed lamellar orders (58).

The X-ray beam was focused by Kirkpatrick–Baez double mirrors and collimated by an aperture to a  $5 \times 5 \mu\text{m}^2$  full-width half-maximum spot at the sample position (59). Longitudinal and transversal sections of Epon-embedded samples were probed in transmission geometry at specific positions using a protein microcrystallography goniometer (58). The sample-to-detector distance was calibrated by an Ag-behenate standard to be 485.3 mm. SAXS patterns were recorded by a MarCCD detector (Rayonix) with typical exposure times of 60 s/pattern. The patterns were displayed and analyzed using the FIT2D software.

## Advanced Neuropathology in DRG Cultures

Following pharmacological manipulation of SP and GP metabolism, DRG cultures were carefully rinsed in DPBS (Gibco, 14190-144), fixed for 20 min in 4% paraformaldehyde (Sigma-Aldrich, P6148) in DPBS, rinsed again in DPBS,

and incubated for 30 min into a permeabilizing/blocking buffer (GSDB buffer) containing 33.3% normal goat serum (DAKO, X0907), 10% Triton-100 (Sigma-Aldrich, T8787), phosphate buffer (240 mM), pH 7.4, and sodium chloride (4 M). Incubation with the anti-myelin basic protein antibody, aa 129–138 clone 1 (Sigma-Aldrich, MAB 382, 1:300), was performed at 4°C in GSDB buffer overnight. After careful rinsing in DPBS, the cells were incubated with Alexa Fluor 594 goat anti-mouse IgG (H+L) secondary antibody (Invitrogen, A11005) at 1:400 dilutions for 1.5 h at 25°C. The cell nuclei were stained with 4',6-diamidino-2-phenylindole dihydrochloride; fluoropure grade (300 nM) (Invitrogen, D1306) and ACLAR dishes were sealed on slides.

Images from the whole DRG culture (80 images/culture and an average number of quantified myelinated internodes of  $1 \times 10^4$ ) were acquired, using the  $\times 20$  objective, with an Olympus PROVIS AX60 microscope connected to an Olympus DP70 digital camera. A morphometric evaluation of the digitized images was performed using an *ad hoc* Image Pro-Plus macro that we recently established in our laboratory, using the Image Pro-Plus Software (Immagini e Computer, Rho, Milan, Italy) (see **Figure S10** and **Video S1**). This semi-automated tool allows a detailed morphometric analysis of the critical parameters for myelinated fibers physiology including (i) myelinated area (i.e., number of myelinated pixels/total pixels on the micrograph) and (ii) internode length and its relative frequency functions. Actually, this allowed us to reliably distinguish CMT1A myelinated internode from the control one for all the parameters analyzed (see **Figure S10**).

## Statistical Analysis

The results are presented as mean  $\pm$  SEM unless otherwise specified. Outliers, whenever present, were identified and removed through the ROUT method ( $Q = 1\%$ ). For myelinated area and internode length, we performed the D'Agostino–Pearson normality test to assess the type of data distribution. Therefore, statistical differences were determined using the non-parametric Mann–Whitney test. For internode length frequency distributions, we performed the non-parametric Kruskal–Wallis test followed by Dunn's multiple-comparisons test. Metabolomics statistics, including PCA, pathway analysis, and volcano plot for the heatmap data, were all performed with MetaboAnalyst software. Statistical differences were considered to be significant when  $P < 0.05$ . Unless otherwise specified, statistical analysis was performed using the Graph Pad 7.0 (Prism) software.

## RESULTS

### SP and GP Pathways Are Mainly Responsible for Lipid Alteration in CMT1A Myelin

To gain a complete overview of CMT1A peripheral nerve lipid composition, we performed a comprehensive lipidomic analysis

both on lipid fraction extracted from sciatic nerve homogenates and on purified myelin.

We found that the CMT1A nerve homogenate displays a distinctive lipid profile compared to that of WT littermates (**Figure 1A**). In particular, we identified 121 lipid species that significantly differ between the two conditions. Among them, SP and GP mostly contributed to this remarkable diversity (**Figures 1B–D**). Notably, the SP and GP species in CMT1A were not merely reduced as it could be expected by the impaired ability of Schwann cells (SCs) to mount the whole lipid biosynthetic transcriptional program during myelination (30); instead we found an incorrect pattern of SP and GP characterized by the presence of lipid species where these were highly increased alongside lipid species where these were extremely decreased (**Figures S1, S2 and Table S1**).

To map this aberrant lipid profile directly into the intact rat sciatic nerve, we performed MALDI-IMS [**Figure S3**; (60)]: the clustering algorithm classified the two genotypes in clearly separate groups just in the endoneurium. Importantly, we also confirmed SP and GP as the most compromised pathways (**Figures S4–S8**).

To unambiguously demonstrate that, among lipids, SP and GP mainly contributed to CMT1A myelin pathology, we performed targeted lipidomics on CMT1A myelin-enriched fraction. Similar to the sciatic nerve, the SP and the GP pathways were deeply altered (**Figures 2A–F**).

Indeed this aberrant lipid composition might also account for the ultrastructural changes of the CMT1A myelin membrane that have been described by us and other groups (29, 30). Thus, to strengthen the issue, we used, for the first time, X-ray diffraction that can precisely detect subtle changes in myelin periodicity to assess both internode myelin quantity and quality in sciatic and sural nerves from CMT1A rats and human patients, respectively (**Figures 2G,H**). Notably, we found a significantly reduced amount of myelin and a substantial widening of myelin period, which are consistent with the aberrant lipid composition [**Figures 2G,H**; (30, 61, 62)].

## Modulation of SP and GP Pathways Affects CMT1A Myelin Physical Structure

To demonstrate a link between SP and GP imbalance and aberrant myelin physical structure in CMT1A, we took advantage from DRG cultures an *in vitro* model of the disease originally developed in our laboratory (29, 45, 63).

In particular, we chronically treated CMT1A and WT DRG cultures with different molecules interfering with both SP and GP metabolism (**Figure 3A**).

We found that four drugs were effective in improving the geometric parameters of CMT1A myelinated fibers (**Figure 3B**). In particular, PtdIns(3,4,5)P3 (PIP3) and lysophosphatidic acid (LPA) were able to significantly increase just the amount of myelinated area without any effect on the internode length (PIP3: 41.5%,  $p < 0.0001$ ; LPA: 65.7%,  $p < 0.0001$ ); conversely, L-serine significantly improved only the internode length (7.5%,  $p < 0.01$ ). Notably, VO-OHpic, a quite specific inhibitor of PTEN,

a phospholipid phosphatase that we found to be significantly increased in CMT1A (**Figure S10**), was able at the same time to positively affect both of these aspects (myelinated area: 48.1%,  $p < 0.01$ ; internode length: 11.9%,  $p < 0.0001$ ). Actually, L-serine and VO-OHpic affected the internode frequency distribution, shifting the function back to the WT condition (**Figure 3B**). Interestingly, when we performed a combined treatment with L-serine and PIP3, we observed an improvement of both internode parameters (myelinated area: 70.3%,  $p < 0.0001$ ; internode length: 11.2%,  $p < 0.0001$ ) following the VO-OHpic treatment, suggesting the existence of at least two independent molecular mechanisms that affect the CMT1A myelin assembly. Notably, these effects did not occur in the WT condition, reinforcing the specificity of CMT1A SP and GP pathway impairment (**Figure 3B**).

## SP and GP Pathways Are a Proper Source of CMT1A Blood Biomarkers

To test whether the massive change of SP and GP metabolism that we found in CMT1A myelin might be traced into the circulatory system, we performed a complete lipid profile in CSF and serum from CMT1A rat and human patients. We identified a unique and specific lipid profile in the CSF of CMT1A rats compared to controls (**Figure 4A**). In particular, we recognized 37 features that clearly discriminate the two experimental groups, as shown in the corresponding heatmap (**Figure S11 and Table S1**). Also, in the rat serum, the CMT1A lipid profile strongly diverged from that of the WT littermates, supporting the notion that a systemic impairment of lipid metabolism is present in this neuropathy (**Figure 4B**). Notably, serum lipidomics in the rat revealed that 67 features, mostly belonging to SP and GP metabolism, especially contributed to the unique lipid profile of CMT1A (**Figure S11 and Table S1**). Owing to the highly consistent results obtained in experimental CMT1A, we extended our study to human subjects by performing lipidomics on the serum collected from 28 genetically defined CMT1A patients and 15 age-matched healthy donors, without any evident comorbidity with diseases that compromise lipid metabolism. As reported in the score plot, the CMT1A patients significantly clustered from healthy controls (**Figure 4C**). In particular, 141 features were dysregulated between the two groups. Once again, the majority of these features belong to SP and GP pathways (**Figure S11 and Table S1**). Interestingly, among them, we found remarkable alterations in the levels of known myelin-enriched lipids, including sulfatides and gangliosides, supporting the notion that the CMT1A lipid perturbation present in peripheral myelin may be tracked in the blood. Of note is the fact that these changes were definitely huge: most of the identified features increased or decreased by more than hundreds of thousands of times in human serum, an optimal condition to perform a future biomarker discovery activity. Indeed the comparative pathway analysis between CMT1A rat and human biological fluids showed that the alteration of SP and GP metabolism was the common feature (**Figures 4D–H**).

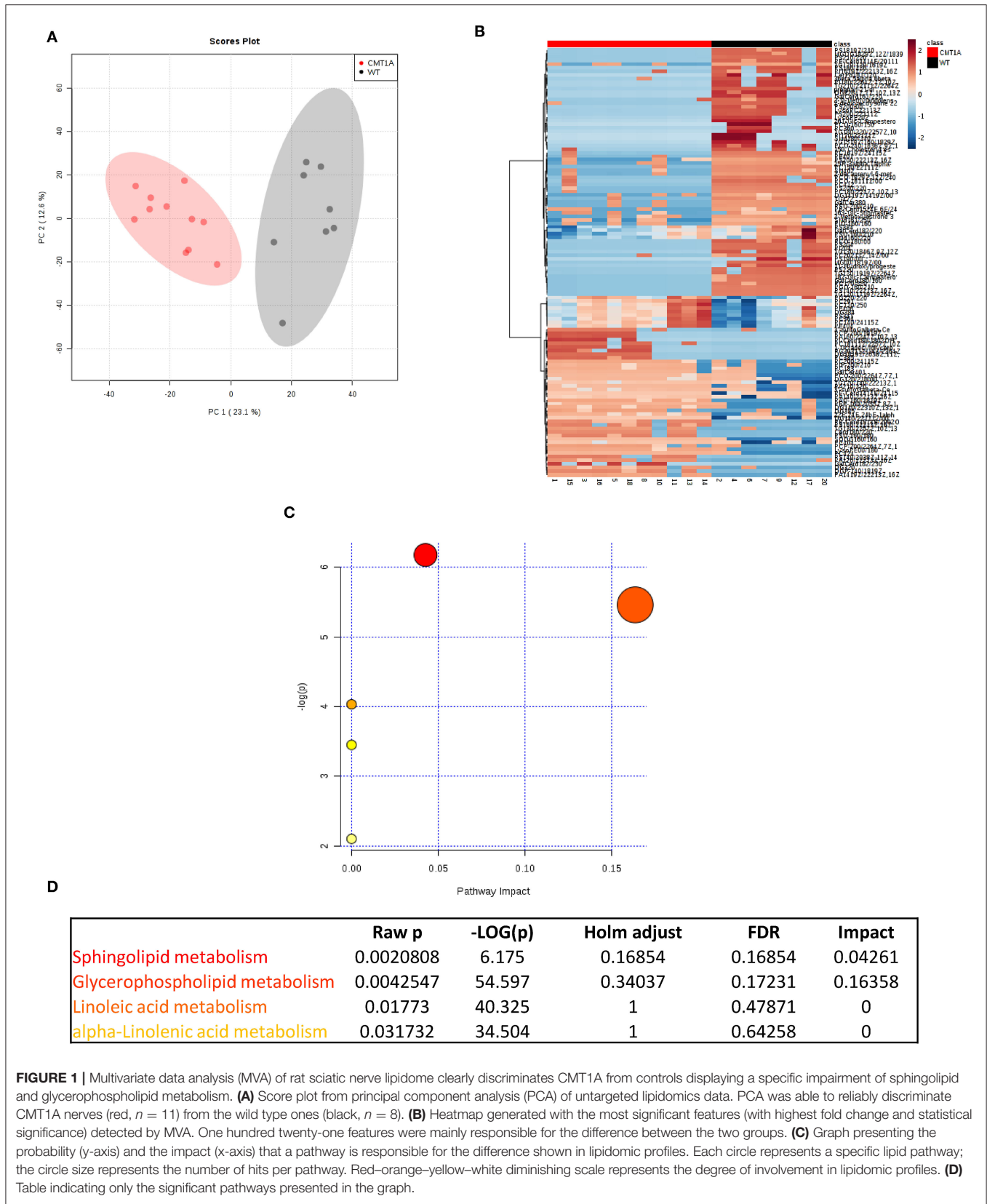


**FIGURE 1 |** Multivariate data analysis (MVA) of rat sciatic nerve lipidome clearly discriminates CMT1A from controls displaying a specific impairment of sphingolipid and glycerophospholipid metabolism. **(A)** Score plot from principal component analysis (PCA) of untargeted lipidomics data. PCA was able to reliably discriminate CMT1A nerves (red,  $n = 11$ ) from the wild type ones (black,  $n = 8$ ). **(B)** Heatmap generated with the most significant features (with highest fold change and statistical significance) detected by MVA. One hundred twenty-one features were mainly responsible for the difference between the two groups. **(C)** Graph presenting the probability (y-axis) and the impact (x-axis) that a pathway is responsible for the difference shown in lipidomic profiles. Each circle represents a specific lipid pathway; the circle size represents the number of hits per pathway. Red–orange–yellow–white diminishing scale represents the degree of involvement in lipidomic profiles. **(D)** Table indicating only the significant pathways presented in the graph.

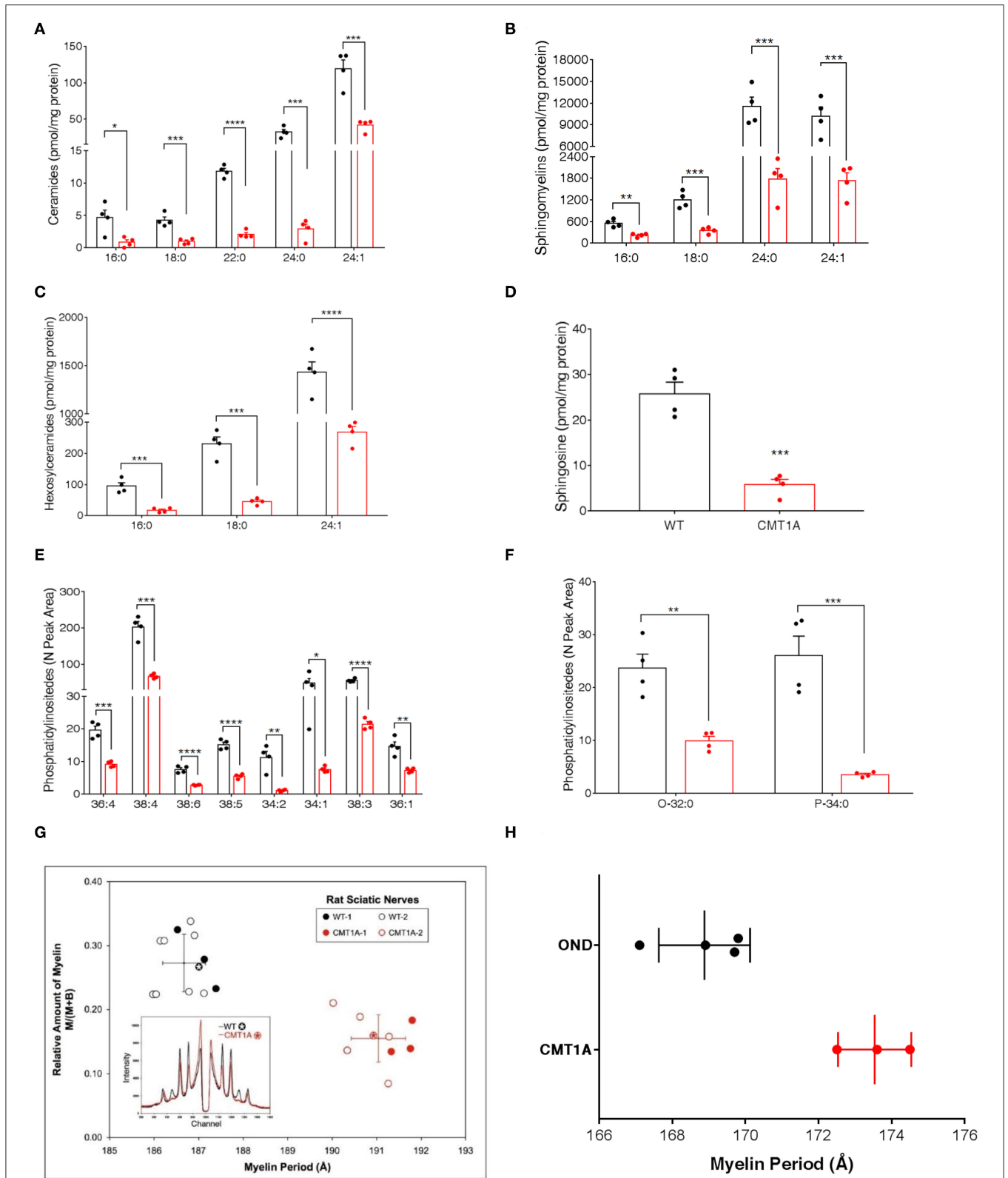


**FIGURE 2 |** CMT1A myelin displayed perturbed sphingolipid (SP) and glycerophospholipid composition and ultrastructural abnormalities. The most abundant SP species were analyzed by an optimized protocol of targeted mass spectrometry. This method uses 25 standards to calculate the absolute concentration (nM) of  
(Continued)

**FIGURE 2** | sphingolipids of interest. **(A–D)** Ceramides, sphingomyelins, hexosylceramides, and sphingosine were all reduced in the CMT1A samples. **(E,F)** Phosphatidylinositides were the lipid species mainly altered in CMT1A myelin by shotgun untargeted analysis. The compound names are presented on the y-axis, while different acyl chains, saturate, or insaturate, are presented on the x-axis. Data are presented as mean  $\pm$  mean of standard error. Wild type (WT) (black), CMT1A (red)  $n = 4$ . Statistics was calculated with unpaired *t*-test, two-tailed. \*\*\*\* $p < 0.0001$ , \*\*\* $p < 0.001$ , \*\* $p < 0.01$ , and \* $p < 0.05$ . **(G)** X-ray diffraction performed on WT and CMT1A rat sciatic nerves from four different litters at 1.5 months (filled symbols) and at 3 months (open symbols) of age. The whole nerves were fixed in 2.5% glutaraldehyde in cacodylate buffer, pH 7.4, for 24 h. In the graph, the relative amount of myelin vs. myelin period is reported. The CMT1A rats showed a significantly reduced myelin content and an enlarged myelin periodicity compared to the WT littermates, which demonstrates the presence of myelin ultrastructural alterations in this neuropathy (WT black,  $n = 12$ ; CMT1A red,  $n = 9$ , unpaired *t*-test, two-tailed;  $p < 0.0001$  for both relative amount of myelin and myelin periodicity). The inset shows examples of the diffraction patterns, expressed as diffracted intensity vs. detector channel number. The patterns correspond to the data points marked by the asterisks. The small shift in the positions of the Bragg peaks indicates differences in periodicity, and the weaker peaks indicate less myelin. The middle region of each pattern, approximate channel numbers 950–1,050, is central scatter from the direct beam around the beam stop and, therefore, is excluded from the analysis. **(H)** X-ray diffraction performed on human sural nerve biopsies of patients affected by CMT1A compared to patients affected by other neurological diseases (OND). The nerves were fixed in buffered glutaraldehyde, processed for electron microscopy, and embedded in Epon, which accounts for the differences in periodicities with the results in **(G)**. Notably, the CMT1A patients (red,  $n = 3$ ) displayed enlarged myelin periodicity compared to the control patients (OND, black,  $n = 4$ , unpaired *t*-test, two-tailed;  $p < 0.01$ ) as was found in the CMT1A rat. Data are presented as mean  $\pm$  standard deviation.

## DISCUSSION

Myelin lipid deficiency and its partial rescue in response to a lipid-enriched diet have been recently shown in the CMT1A rat model (30).

The present study provides evidence for the first time that, following a comprehensive analysis of the whole lipidome, just SP and GP are responsible for the CMT1A perturbed lipid metabolism in the nerve, myelin, and biological fluids.

These results definitely extend and better define earlier works (30, 39). Of note also in our study is that different SP and GP species (including phosphatidylcholines) are altered in CMT1A, but with species increased as well as decreased, complicating the issue. In this context, it is well-known that the unique lipid stoichiometry of myelin directly influences its ultrastructure and physiology, thereby regulating nerve conduction (26, 31). In fact, myelin is subjected to different physical and functional rearrangements during development, including progressive thickening, lengthening along fiber internodes, and increasing of conduction velocity. All these features are altered in CMT1A and never reach normal values (64–68). Indeed changes in CMT1A myelin geometric parameters have already been shown by us and other groups (29, 30, 64, 69). Moreover, here we demonstrate by X-ray diffraction analysis a flawed physical structure of internode myelin in both experimental and human CMT1A.

To link SP and GP imbalance with CMT1A myelin architecture, we investigated the morphometric changes of the myelinated internode in DRG cultures treated with different molecules affecting just these lipid pathways (32, 70–79). Of note is that most of the SP and GP species displaying a greater change do not only have a structural role in myelin but are also able to impact on signaling and transcription itself (34).

Among all the tested molecules, we found that L-serine, PIP3, LPA, and VO-OHPic were able to improve CMT1A myelin internode, in contrast to an earlier work in which lipid supplement was unable to influence these parameters (30). Moreover, the effect of our treatments was specific for the CMT1A condition as we did not observe any effect in wild-type cultures.

Indeed these molecules deeply interfere with normal and pathological myelination. In fact, L-serine is a key polar amino acid required for SP synthesis, being an essential substrate for SPTLC1, the rate-limiting enzyme of SP metabolism; peripheral

myelin is particularly sensitive to SP composition and change (80, 81). PIP3, in glia, triggers autonomous cell wrapping during myelination, and an imbalance of PIP homeostasis is at the basis of altered longitudinal myelin growth and myelin outfolding formation (37, 73, 82, 83). LPA is an early precursor of PI that regulates crucial signaling in myelin, including embryonic SC migration, myelination, and cell-to-axon segregation; PI also prevents SC apoptosis through activation of PI3K, a key enzyme for PIP3 homeostasis (70). Finally, VO-OHPic is a synthetic specific inhibitor of PTEN, an enzyme that works in concert with Dlg1 as myelination inhibitor, and deletion of PTEN in adult SCs is able to reactivate myelin growth (77, 84, 85).

We would like to highlight that these molecules act on the PI3K/PTEN pathway, a well-known CMT1A hub, downstream to NRG1, further sustaining the importance of SP and GP metabolism in myelin development and maintenance.

We found that these molecules affect myelinated area and internode length in different ways: in fact, while PIP3 and LPA significantly increased the amount of myelinated fibers without any effect on their structure, L-serine and VO-OHPic just increased the internode length, suggesting the existence of at least two independent mechanisms essential for correct myelination. This hypothesis is further strengthened by the cumulative effect of PIP3 and L-serine simultaneous administration, which was able to improve both the quantity and the quality of the myelin internode.

Trying to further explain our results, we envisage that these treatments are able to impact on SC differentiation and proliferation, two biological processes highly compromised in CMT1A (86, 87). Indeed LPA and PIP3, improving the myelinated area through the PI3K/PTEN pathway, may directly trigger the CMT1A SC differentiation program (70, 73). The positive effect of L-serine and VO-OHPic on CMT1A internode length might instead be due to their ability to inhibit proliferation. In fact, the relation between increased proliferation and shortening of internode is well-known (88–90). Interestingly, several studies demonstrate that SPTLC1 and PTEN, sensitive to L-serine, and VO-OHPic, respectively, are also able to modulate proliferation independently from their normal enzymatic activity (91–93). Further studies are needed to demonstrate the correlation between abnormal cellular proliferation and myelin structure impairment in CMT1A.

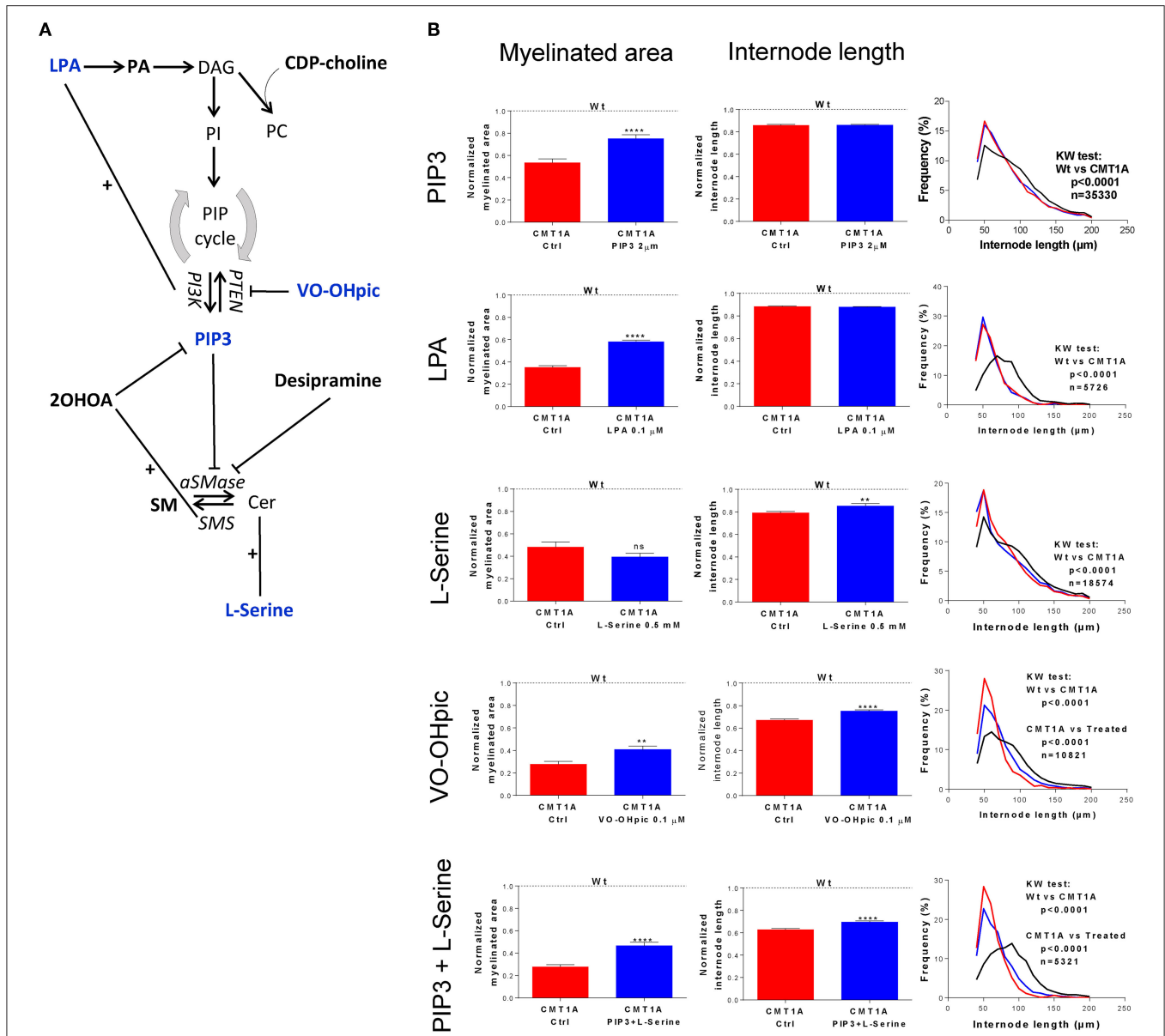


**FIGURE 3 |** Modulation of sphingolipid (SP) and glycerophospholipid (GP) pathways affects the CMT1A myelin physical structure. **(A)** Schematic illustration of treatment schedule adopted to demonstrate the specific involvement of SP and GP in CMT1A myelinopathy. The CMT1A and WT DRG cultures were chronically treated with several molecules selected for their proven efficacy on SP and GP pathway modulation in the presence of 15% newborn calf serum, ascorbic acid (100 μg/ml final concentration), and nerve growth factor at 5 ng/ml final concentration. In particular, we analyzed the effects on myelination of LPA, PA, CDP-choline, PIP3, VO-OHpic, 2OHOA, desipramine, SM, and L-serine. **(B)** Advanced neuropathology (see also the **Video S1**) performed on dorsal root ganglia (DRG) myelinated fibers allowed us to select PIP3, LPA, VO-OHpic, and L-serine as the most effective molecules. Interestingly, we found that these molecules improved the CMT1A myelinopathy—a reduced amount of myelinated fibers and shortening of the internode length—in a different way. In fact, while PIP3 and LPA significantly increased the amount of myelinated fibers without any effect on their structure [CMT1A Ctrl (*n* = 180) vs. CMT1A PIP3 (*n* = 215), mean ± SD: 0.53 ± 0.43 vs. 0.75 ± 0.50; CMT1A Ctrl (*n* = 405) vs. CMT1A LPA (*n* = 511), mean ± SD: 0.35 ± 0.27 vs. 0.58 ± 0.40], L-serine and VO-OHpic just increased the internode length [CMT1A Ctrl (*n* = 102) vs. CMT1A L-serine (*n* = 113), mean ± SD: 0.79 ± 0.12 vs. 0.85 ± 0.23; CMT1A Ctrl (*n* = 128) vs. CMT1A VO-OHpic (*n* = 155), mean ± SD: 0.67 ± 0.11 vs. 0.75 ± 0.11], suggesting the existence of at least two independent mechanisms essential for correct myelination. This hypothesis is further strengthened by the cumulative effect of PIP3 and L-serine simultaneous administration to CMT1A DRG cultures, which was able to improve both the quantity and the quality of pathological myelin [CMT1A Ctrl (*n* = 112) vs. CMT1A PIP3+L-serine (*n* = 145), myelinated area mean ± SD: 0.27 ± 0.20 vs. 0.46 ± 0.36; CMT1A Ctrl (*n* = 112) vs. CMT1A PIP3+L-serine (*n* = 145), internode length mean ± SD: 0.62 ± 0.10 vs. 0.69 ± 0.12]. LPA, lysophosphatidic acid; PA, phosphatidic acid; DAG, diacylglycerol; CDP-choline, cytidine-5′-diphospho-choline; PI, phosphoinositide; PC, phosphatidylcholine; PIP, phosphatidylinositol phosphate; PTEN, phosphatase and tensin homolog; VO-OHpic, a PTEN inhibitor; PI3K, phosphatidylinositol-3-kinase; PIP3, phosphatidylinositol tris-3,4,5-phosphate; 2OHOA, 2-hydroxy oleic acid; SM, sphingomyelin; aSMase, acid sphingomyelinase; SMS, sphingomyelin synthase; Cer, ceramide. For myelinated area and internode length, we performed the D’Agostino–Pearson normality test to assess the type of data distribution. Therefore, statistical differences were determined using the non-parametric Mann–Whitney test (*n* represents the number of analyzed images in at least three biological replicates). For internode length frequency distributions, we performed non-parametric Kruskal–Wallis test followed by Dunn’s multiple-comparisons test (*n* represents the total number of analyzed internodes). ns, not significant; \*\**p* < 0.01 and \*\*\*\**p* < 0.0001.

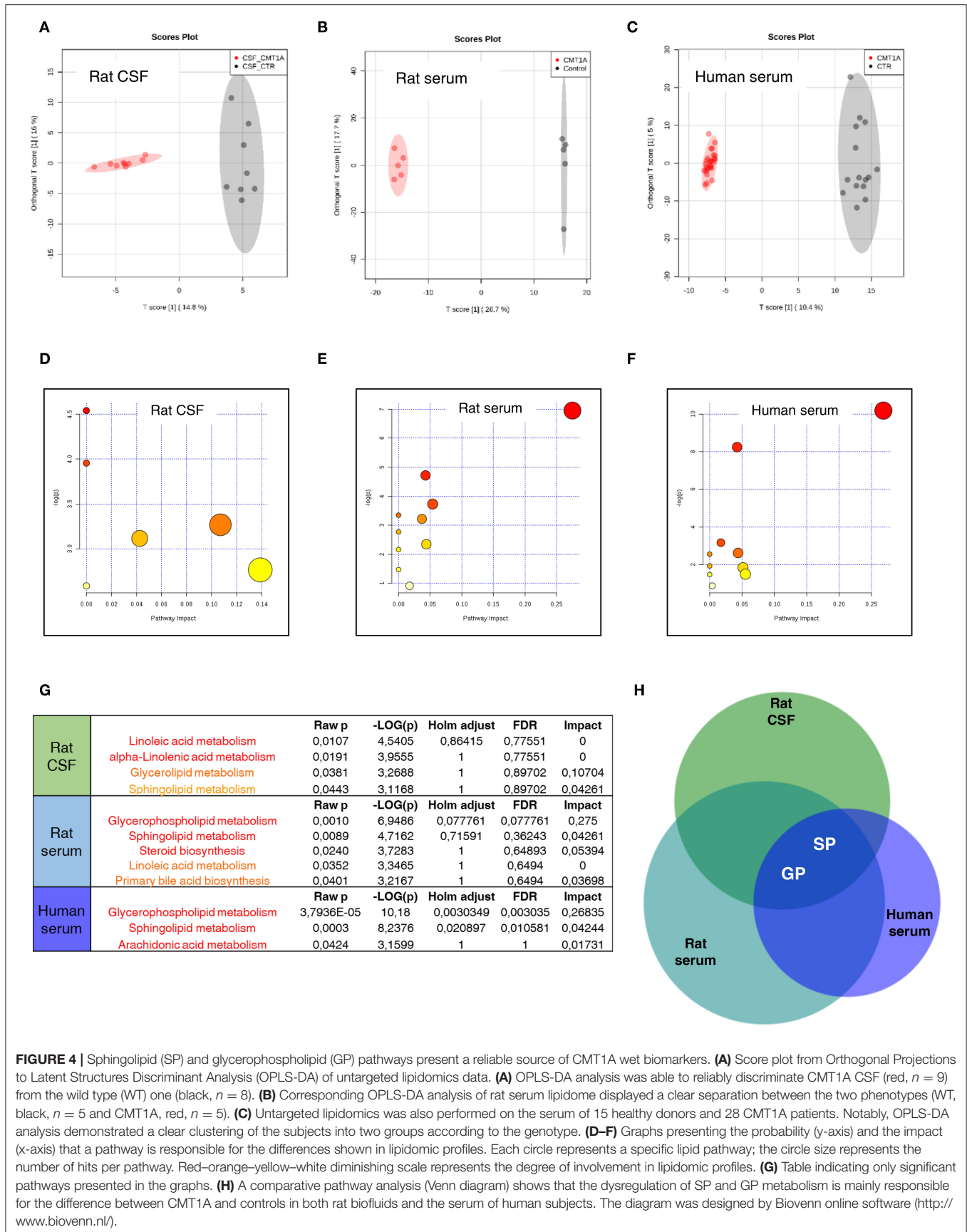


**FIGURE 4 |** Spingolipid (SP) and glycerophospholipid (GP) pathways present a reliable source of CMT1A wet biomarkers. **(A)** Score plot from Orthogonal Projections to Latent Structures Discriminant Analysis (OPLS-DA) of untargeted lipidomics data. **(A)** OPLS-DA analysis was able to reliably discriminate CMT1A CSF (red,  $n = 9$ ) from the wild type (WT) one (black,  $n = 8$ ). **(B)** Corresponding OPLS-DA analysis of rat serum lipidome displayed a clear separation between the two phenotypes (WT, black,  $n = 5$  and CMT1A, red,  $n = 5$ ). **(C)** Untargeted lipidomics was also performed on the serum of 15 healthy donors and 28 CMT1A patients. Notably, OPLS-DA analysis demonstrated a clear clustering of the subjects into two groups according to the genotype. **(D–F)** Graphs presenting the probability (y-axis) and the impact (x-axis) that a pathway is responsible for the differences shown in lipidomic profiles. Each circle represents a specific lipid pathway; the circle size represents the number of hits per pathway. Red–orange–yellow–white diminishing scale represents the degree of involvement in lipidomic profiles. **(G)** Table indicating only significant pathways presented in the graphs. **(H)** A comparative pathway analysis (Venn diagram) shows that the dysregulation of SP and GP metabolism is mainly responsible for the difference between CMT1A and controls in both rat biofluids and the serum of human subjects. The diagram was designed by Biovenn online software (<http://www.biovenn.nl/>).

Overall, our results display a leading role of SP and GP metabolism in CMT1A impaired myelination.

Notably, the same SP and GP dysregulation emerges from the lipidomics performed on biological fluids both in experimental and in human CMT1A. Our results strongly recommend SP and GP as a promising source of disease biomarkers. Actually, while there is no need for CMT1A diagnostic biomarkers, great effort is underway to identify disease severity biomarkers to stage patients, to follow disease progression, and to monitor drug efficacy in clinical trials (94). To date, transcriptional biomarkers in skin biopsies of experimental and human CMT1A have been proposed, demonstrating that disease severity can be related to cutaneous mRNA expression (14, 95). Moreover, a study performed on the plasma of CMT1A patients highlighted an increase of protein catabolism and the mobilization of membrane lipids involved in inflammatory signaling as further potential sources of biomarkers (96). Nevertheless, we are still far from having reliable and clinically acceptable disease severity biomarkers. Owing to our analysis of the CMT1A serum lipid profile, a most reliable fluid in clinical practice, it is our opinion that the present study represents a critical step toward this direction.

Finally, despite that our study is focused on CMT1A, it is intriguing that defects of lipid metabolism have been described in several other peripheral neuropathies. Among them, there are not only inherited dysmyelinating CMT—including CMT1B, CMT4B1, and CMT4J—but also HSN type 1 and diabetic neuropathy (37, 97–100). Even some axonal CMT2 neuropathies display a dysregulation of lipid metabolism, which further supports a critical role of bioactive lipid species in peripheral nerve physiology (42, 101).

## CONCLUSIONS

The lipidome profiling in experimental and in human CMT1A reported herein for the first time and the established previously unknown alterations in SP and GP metabolism expand the spectrum of molecular changes in CMT1A. The consistent systemic altered lipidome of affected patients deeply supports the use of lipid serum biomarkers in CMT1A and possibly other CMT neuropathies in which lipid biosynthesis and myelin remodeling are compromised. These novel data provide insights into the pathological alterations in the CMT1A neuropathy at a molecular level and could potentially contribute to the development of novel disease-modifying approaches.

## DATA AVAILABILITY STATEMENT

All datasets generated for this study are included in the article/**Supplementary Material**. Raw data are available from the corresponding author on reasonable request.

## ETHICS STATEMENT

The studies involving human participants were reviewed and approved by the Regional Ethics Committee (CER Liguria) (project number approval 545REG2015). The

patients/participants provided their written informed consent to participate in this study. The animal study was reviewed and approved by the OPBA (Institutional Animal Welfare Body) and the Italian Ministry of Health (project number approval 798/2016-PR).

## AUTHOR CONTRIBUTIONS

DV and GC planned the experiments and analyzed the data. DV wrote the manuscript. GC performed immunohistochemistry on DRG cultures and supervised the serum collection from human patients. DM and CP prepared the samples for the analyses from animal material. AB and ZH acquired targeted and untargeted lipidomic data. BP did sample preparation and the MALDI-IMS experimental work. RF performed the MALDI-IMS data analysis and lipid identification. CG enrolled patients and collected the serum samples and clinical data. JF coordinated the MALDI-IMS experiments and took part in the interpretation. CR performed the X-ray scattering experiments at the ESRF and analyzed the data. DK and AL undertook the small-angle X-ray diffraction on aldehyde-fixed nerves and analyzed the data. DK contributed to the writing of the manuscript. AS contributed to the manuscript discussion. AA contributed to the LC-MS/MS experimental design and data analysis. LN designed and supervised the study, performed and analyzed the experiments on DRG cultures, and wrote the manuscript. All authors contributed to the article and approved the submitted version.

## FUNDING

This study was supported by FISM—Fondazione Italiana Sclerosi Multipla—cod. 2015/R/17 to LN, PRA—Progetti di Ricerca di Ateneo—University of Genoa, Italy to AS, and Kedrion S.p.A. The X-ray experiments in the Kirschner Lab were supported by institutional research funds from Boston College. JF thanks the Spanish Ministry of Economy and Competitiveness, grant RTC-2015-3693-1 (RETOS program), co-financed by Fondo Europeo de Desarrollo regional (FEDER) EU for economic support and to the *Servicio de Lipidómica* of the SGIKER (UPV/EHU, MINECO, GV/EJ, ESF) for its technical and human support.

## ACKNOWLEDGMENTS

We are in debt with the specialists of the CMT Clinic of our department for their collaboration in collecting serum samples from human patients and healthy donors. The X-ray experiments in the Kirschner lab were carried out in part by Michelle N. Crowther (BC'10).

## SUPPLEMENTARY MATERIAL

The Supplementary Material for this article can be found online at: <https://www.frontiersin.org/articles/10.3389/fneur.2020.00903/full#supplementary-material>

## REFERENCES

- Brennan KM, Bai Y, Shy ME. Demyelinating CMT—what's known, what's new and what's in store? *Neurosci Lett.* (2015) 596:14–26. doi: 10.1016/j.neulet.2015.01.059
- Mathis S, Goizet C, Tazir M, Magdelaine C, Lia AS, Magy L, et al. Charcot-Marie-Tooth diseases: an update and some new proposals for the classification. *J Med Genet.* (2015) 52:681–90. doi: 10.1136/jmedgenet-2015-103272
- Timmerman V, Nelis E, Van Hul W, Nieuwenhuijsen BW, Chen KL, Wang S, et al. The peripheral myelin protein gene PMP-22 is contained within the Charcot-Marie-Tooth disease type 1A duplication. *Nat Genet.* (1992) 1:171–5. doi: 10.1038/ng0692-171
- Patel PI, Roa BB, Welcher AA, Schoener-Scott R, Trask BJ, Pentao L, et al. The gene for the peripheral myelin protein PMP-22 is a candidate for Charcot-Marie-Tooth disease type 1A. *Nat Genet.* (1992) 1:159–65. doi: 10.1038/ng0692-159
- Schenone A, Nobbio L, Monti Bragadin M, Ursino G, Grandis M. Inherited neuropathies. *Curr Treat Options Neurol.* (2011) 13:160–79. doi: 10.1007/s11940-011-0115-z
- Roa BB, Garcia CA, Lupski JR. Charcot-Marie-Tooth disease type 1A: molecular mechanisms of gene dosage and point mutation underlying a common inherited peripheral neuropathy. *Int J Neurol.* (1991) 25–26:97–107.
- Nobbio L, Visigalli D, Radice D, Fiorina E, Solari A, Lauria G, et al. PMP22 messenger RNA levels in skin biopsies: testing the effectiveness of a Charcot-Marie-Tooth 1A biomarker. *Brain.* (2014) 137(Pt 6):1614–20. doi: 10.1093/brain/awu071
- Li J. Caveats in the Established Understanding of CMT1A. *Ann Clin Transl Neurol.* (2017) 4:601–7. doi: 10.1002/acn3.432
- Tao F, Beecham GW, Rebelo AP, Blanton SH, Moran JJ, Lopez-Anido C, et al. Modifier gene candidates in Charcot-Marie-Tooth disease type 1A: a case-only genome-wide association study. *J Neuromuscul Dis.* (2019) 6:201–11. doi: 10.3233/JND-190377
- Tao F, Beecham GW, Rebelo AP, Svaren J, Blanton SH, Moran JJ, et al. Variation in SIPA1L2 is correlated with phenotype modification in Charcot-Marie-Tooth disease type 1A. *Ann Neurol.* (2019) 85:316–30. doi: 10.1002/ana.25426
- Tao F, Inherited Neuropathy C, Zuchner S. Replication studies of MIR149 association in Charcot-Marie-Tooth disease type 1A in a European population. *Neuromuscul Disord.* (2019) 29:160–2. doi: 10.1016/j.nmd.2018.12.012
- Pantera H, Shy ME, Svaren J. Regulating PMP22 expression as a dosage sensitive neuropathy gene. *Brain Res.* (2020) 1726:146491. doi: 10.1016/j.brainres.2019.146491
- Serfecz J, Bazick H, Al Salihi MO, Turner P, Fields C, Cruz P, et al. Downregulation of the human peripheral myelin protein 22 gene by miR-29a in cellular models of Charcot-Marie-Tooth disease. *Gene Ther.* (2019) 26:455–64. doi: 10.1038/s41434-019-0098-z
- Svaren J, Moran JJ, Wu X, Zuccharino R, Bacon C, Bai Y, et al. Schwann cell transcript biomarkers for hereditary neuropathy skin biopsies. *Ann Neurol.* (2019) 85:887–98. doi: 10.1002/ana.25480
- Lee JS, Lee JY, Song DW, Bae HS, Doo HM, Yu HS, et al. Targeted PMP22 TATA-box editing by CRISPR/Cas9 reduces demyelinating neuropathy of Charcot-Marie-Tooth disease type 1A in mice. *Nucleic Acids Res.* (2019) 48:130–40. doi: 10.1093/nar/gkz1070
- Zhao HT, Damle S, Ikeda-Lee K, Kuntz S, Li J, Mohan A, et al. PMP22 antisense oligonucleotides reverse Charcot-Marie-Tooth disease type 1A features in rodent models. *J Clin Invest.* (2018) 128:359–68. doi: 10.1172/JCI96499
- Lewis RA, McDermott MP, Herrmann DN, Hoke A, Clawson LL, Siskind C, et al. High-dosage ascorbic acid treatment in Charcot-Marie-Tooth disease type 1A: results of a randomized, double-masked, controlled trial. *JAMA Neurol.* (2013) 70:981–7. doi: 10.1001/jamaneurol.2013.3178
- Pareyson D, Marchesi C. Diagnosis, natural history, and management of Charcot-Marie-Tooth disease. *Lancet Neurol.* (2009) 8:654–67. doi: 10.1016/S1474-4422(09)70110-3
- Chandran JS, Scarrott JM, Shaw PJ, Azzouz M. Gene therapy in the nervous system: failures and successes. *Adv Exp Med Biol.* (2017) 1007:241–57. doi: 10.1007/978-3-319-60733-7\_13
- Juneja M, Burns J, Saporta MA, Timmerman V. Challenges in modelling the Charcot-Marie-Tooth neuropathies for therapy development. *J Neurol Neurosurg Psychiatry.* (2018) 90:58–67. doi: 10.1136/jnnp-2018-318834
- Visigalli D, Castagnola P, Capodivento G, Geroldi A, Bellone E, Mancardi G, et al. Alternative splicing in the human PMP22 gene: implications in CMT1A neuropathy. *Hum Mutat.* (2016) 37:98–109. doi: 10.1002/humu.22921
- Sereda MW, Meyer zu Horste G, Suter U, Uzma N, Nave KA. Therapeutic administration of progesterone antagonist in a model of Charcot-Marie-Tooth disease (CMT-1A) *Nat Med.* (2003) 9:1533–7. doi: 10.1038/nm957
- Sociali G, Visigalli D, Prukop T, Cervellini I, Mannino E, Venturi C, et al. Tolerability and efficacy study of P2X7 inhibition in experimental Charcot-Marie-Tooth type 1A (CMT1A) neuropathy. *Neurobiol Dis.* (2016) 95:145–57. doi: 10.1016/j.nbd.2016.07.017
- Chumakov I, Milet A, Cholet N, Primas G, Boucard A, Pereira Y, et al. Polytherapy with a combination of three repurposed drugs (PXT3003) down-regulates Pmp22 over-expression and improves myelination, axonal and functional parameters in models of CMT1A neuropathy. *Orphanet J Rare Dis.* (2014) 9:201. doi: 10.1186/s13023-014-0201-x
- Fledrich R, Stassart RM, Klink A, Rasch LM, Prukop T, Haag L, et al. Soluble neuregulin-1 modulates disease pathogenesis in rodent models of Charcot-Marie-Tooth disease 1A. *Nat Med.* (2014) 20:1055–61. doi: 10.1038/nm.3664
- Schmitt S, Castelvetti LC, Simons M. Metabolism and functions of lipids in myelin. *Biochim Biophys Acta.* (2015) 1851:999–1005. doi: 10.1016/j.bbali.2014.12.016
- Court FA, Sherman DL, Pratt T, Garry EM, Ribchester RR, Cottrell DF, et al. Restricted growth of Schwann cells lacking Cajal bands slows conduction in myelinated nerves. *Nature.* (2004) 431:191–5. doi: 10.1038/nature02841
- Hu B, Arpag S, Zhang X, Mobius W, Werner H, Sosinsky G, et al. Tuning PAK activity to rescue abnormal myelin permeability in HNPP. *PLoS Genet.* (2016) 12:e1006290. doi: 10.1371/journal.pgen.1006290
- Nobbio L, Mancardi G, Grandis M, Levi G, Suter U, Nave KA, et al. PMP22 transgenic dorsal root ganglia cultures show myelin abnormalities similar to those of human CMT1A. *Ann Neurol.* (2001) 50:47–55. doi: 10.1002/ana.1034
- Fledrich R, Abdelaal T, Rasch L, Bansal V, Schutz V, Brugger B, et al. Targeting myelin lipid metabolism as a potential therapeutic strategy in a model of CMT1A neuropathy. *Nat Commun.* (2018) 9:3025. doi: 10.1038/s41467-018-05420-0
- Li J. Molecular regulators of nerve conduction - Lessons from inherited neuropathies and rodent genetic models. *Exp Neurol.* (2015) 267:209–18. doi: 10.1016/j.expneurol.2015.03.009
- Capodivento G, Visigalli D, Garnerio M, Fancellu R, Ferrara MD, Basit A, et al. Sphingomyelin as a myelin biomarker in CSF of acquired demyelinating neuropathies. *Sci Rep.* (2017) 7:7831. doi: 10.1038/s41598-017-08314-1
- da Silva TE, Eira J, Lopes AT, Malheiro AR, Sousa V, Luoma A, et al. Peripheral nervous system plasmalogens regulate Schwann cell differentiation and myelination. *J Clin Invest.* (2014) 124:2560–70. doi: 10.1172/JCI72063
- Chrast R, Saher G, Nave KA, Verheijen MH. Lipid metabolism in myelinating glial cells: lessons from human inherited disorders and mouse models. *J Lipid Res.* (2011) 52:419–34. doi: 10.1194/jlr.R009761
- Landrieu P, Said G. Peripheral neuropathy in type A Niemann-Pick disease. A morphological study. *Acta Neuropathol.* (1984) 63:66–71.
- Matsumoto R, Oka N, Nagahama Y, Akiguchi I, Kimura J. Peripheral neuropathy in late-onset Krabbe's disease: histochemical and ultrastructural findings. *Acta Neuropathol.* (1996) 92:635–9.
- Vaccari I, Dina G, Tronchere H, Kaufman E, Chicanne G, Cerri F, et al. Genetic interaction between MTMR2 and FIG4 phospholipid phosphatases involved in Charcot-Marie-Tooth neuropathies. *PLoS Genet.* (2011) 7:e1002319. doi: 10.1371/journal.pgen.1002319
- Sahu SK, Hannun YA, Yao N. Emergence of membrane sphingolipids as a potential therapeutic target. *Biochimie.* (2019) 158:257–64. doi: 10.1016/j.biochi.2019.01.018
- Zhou Y, Bazick H, Miles JR, Fethiere AI, Salihi MOA, Fazio S, et al. A neutral lipid-enriched diet improves myelination and alleviates

- peripheral nerve pathology in neuropathic mice. *Exp Neurol.* (2019) 321:113031. doi: 10.1016/j.expneurol.2019.113031
40. Mapstone M, Cheema AK, Fiandaca MS, Zhong X, Mhyre TR, MacArthur LH, et al. Plasma phospholipids identify antecedent memory impairment in older adults. *Nat Med.* (2014) 20:415–8. doi: 10.1038/nm.3466
  41. Quintana FJ, Yeste A, Weiner HL, Covacu R. Lipids and lipid-reactive antibodies as biomarkers for multiple sclerosis. *J Neuroimmunol.* (2012) 248:53–7. doi: 10.1016/j.jneuroim.2012.01.002
  42. Atkinson D, Nikodinovic Glumac J, Asselbergh B, Ermanoska B, Blocquel D, Steiner R, et al. Sphingosine 1-phosphate lyase deficiency causes Charcot-Marie-Tooth neuropathy. *Neurology.* (2017) 88:533–42. doi: 10.1212/WNL.0000000000003595
  43. van Meer G. Cellular lipidomics. *EMBO J.* (2005) 24:3159–65. doi: 10.1038/sj.emboj.7600798
  44. Sereda M, Griffiths I, Puhlhofer A, Stewart H, Rossner MJ, Zimmerman F, et al. A transgenic rat model of Charcot-Marie-Tooth disease. *Neuron.* (1996) 16:1049–60.
  45. Nobbio L, Gherardi G, Vigo T, Passalacqua M, Melloni E, Abbruzzese M, et al. Axonal damage and demyelination in long-term dorsal root ganglia cultures from a rat model of Charcot-Marie-Tooth type 1A disease. *Eur J Neurosci.* (2006) 23:1445–52. doi: 10.1111/j.1460-9568.2006.04666.x
  46. Nobbio L, Fiorese F, Vigo T, Cilli M, Gherardi G, Grandis M, et al. Impaired expression of ciliary neurotrophic factor in Charcot-Marie-Tooth type 1A neuropathy. *J Neuropathol Exp Neurol.* (2009) 68:441–55. doi: 10.1097/NEN.0b013e31819fa6ba
  47. Nobbio L, Sturla L, Fiorese F, Usai C, Basile G, Moreschi I, et al. P2X7-mediated increased intracellular calcium causes functional derangement in Schwann cells from rats with CMT1A neuropathy. *J Biol Chem.* (2009) 284:23146–58. doi: 10.1074/jbc.M109.027128
  48. Fridman V, Bundy B, Reilly MM, Pareyson D, Bacon C, Burns J, et al. CMT subtypes and disease burden in patients enrolled in the Inherited Neuropathies Consortium natural history study: a cross-sectional analysis. *J Neurol Neurosurg Psychiatry.* (2015) 86:873–8. doi: 10.1136/jnnp-2014-308826
  49. Larocca JN, Norton WT. Isolation of myelin. *Curr Protoc Cell Biol.* (2007) Chapter 3:Unit 3.25. doi: 10.1002/0471143030.cb0325s33
  50. Liu L, Duff K. A technique for serial collection of cerebrospinal fluid from the cisterna magna in mouse. *J Vis Exp.* (2008) 10:960. doi: 10.3791/960
  51. Bligh EG, Dyer WJ. A rapid method of total lipid extraction and purification. *Can J Biochem Physiol.* (1959) 37:911–7. doi: 10.1139/o59-099
  52. Armirotti A, Basit A, Realini N, Caltagirone C, Bossu P, Spalletta G, et al. Sample preparation and orthogonal chromatography for broad polarity range plasma metabolomics: application to human subjects with neurodegenerative dementia. *Anal Biochem.* (2014) 455:48–54. doi: 10.1016/j.ab.2014.03.019
  53. Geng L, Sun H, Yuan Y, Liu Z, Cui Y, Bi K, et al. Discrimination of raw and vinegar-processed Genkwa Flos using metabolomics coupled with multivariate data analysis: a discrimination study with metabolomics coupled with PCA. *Fitoterapia.* (2013) 84:286–94. doi: 10.1016/j.fitote.2012.12.003
  54. Chong J, Soufan O, Li C, Caraus I, Li S, Bourque G, et al. MetaboAnalyst 4.0: towards more transparent and integrative metabolomics analysis. *Nucleic Acids Res.* (2018) 46:W486–94. doi: 10.1093/nar/gky310
  55. Cajka T, Fiehn O. Comprehensive analysis of lipids in biological systems by liquid chromatography-mass spectrometry. *Trends Analyt Chem.* (2014) 61:192–206. doi: 10.1016/j.trac.2014.04.017
  56. Avila RL, Inouye H, Baek RC, Yin X, Trapp BD, Feltri ML, et al. Structure and stability of internodal myelin in mouse models of hereditary neuropathy. *J Neuropathol Exp Neurol.* (2005) 64:976–90. doi: 10.1097/01.jnen.0000186925.95957.dc
  57. Kirschner DA, Hollingshead CJ. Processing for electron microscopy alters membrane structure and packing in myelin. *J Ultrastruct Res.* (1980) 73:211–32.
  58. Perrakis A, Cipriani F, Castagna JC, Claustre L, Burghammer M, Riekel C, et al. Protein microcrystals and the design of a microdiffractometer: current experience and plans at EMBL and ESRF/ID13. *Acta Crystallogr D Biol Crystallogr.* (1999) 55(Pt 10):1765–70.
  59. Kirkpatrick P, Baez AV. Formation of optical images by X-rays. *J Opt Soc Am.* (1948) 38:766–74. doi: 10.1364/josa.38.000766
  60. Fernandez R, Carriel V, Lage S, Garate J, Diez-Garcia J, Ochoa B, et al. Deciphering the lipid architecture of the rat sciatic nerve using imaging mass spectrometry. *ACS Chem Neurosci.* (2016) 7:624–32. doi: 10.1021/acschemneuro.6b00010
  61. Hayashi A, Kaneko N, Tomihira C, Baba H. Sulfatide decrease in myelin influences formation of the paranodal axo-glia junction and conduction velocity in the sciatic nerve. *Glia.* (2013) 61:466–74. doi: 10.1002/glia.22447
  62. Honke K, Hirahara Y, Dupree J, Suzuki K, Popko B, Fukushima K, et al. Paranodal junction formation and spermatogenesis require sulfoglycolipids. *Proc Natl Acad Sci USA.* (2002) 99:4227–32. doi: 10.1073/pnas.032068299
  63. Nobbio L, Vigo T, Abbruzzese M, Levi G, Brancolini C, Mantero S, et al. Impairment of PMP22 transgenic Schwann cells differentiation in culture: implications for Charcot-Marie-Tooth type 1A disease. *Neurobiol Dis.* (2004) 16:263–73. doi: 10.1016/j.nbd.2004.02.007
  64. Saporita MA, Katona I, Lewis RA, Masse S, Shy ME, Li J. Shortened internodal length of dermal myelinated nerve fibres in Charcot-Marie-Tooth disease type 1A. *Brain.* (2009) 132(Pt 12):3263–73. doi: 10.1093/brain/awp274
  65. Friede RL, Brzoska J, Hartmann U. Changes in myelin sheath thickness and internode geometry in the rabbit phrenic nerve during growth. *J Anat.* (1985) 143:103–13.
  66. Garcia A, Combarros O, Calleja J, Berciano J. Charcot-Marie-Tooth disease type 1A with 17p duplication in infancy and early childhood: a longitudinal clinical and electrophysiologic study. *Neurology.* (1998) 50:1061–7.
  67. Manganelli F, Pisciotto C, Reilly MM, Tozza S, Schenone A, Fabrizi GM, et al. Nerve conduction velocity in CMT1A: what else can we tell? *Eur J Neurol.* (2016) 23:1566–71. doi: 10.1111/ene.13079
  68. Manganelli F, Nolano M, Pisciotto C, Provitera V, Fabrizi GM, Cavallaro T, et al. Charcot-Marie-Tooth disease: new insights from skin biopsy. *Neurology.* (2015) 85:1202–8. doi: 10.1212/WNL.0000000000001993
  69. Rangaraju S, Verrier JD, Madorsky I, Nicks J, Dunn WA Jr, Notterpek L. Rapamycin activates autophagy and improves myelination in explant cultures from neuropathic mice. *J Neurosci.* (2010) 30:11388–97. doi: 10.1523/JNEUROSCI.1356-10.2010
  70. Anliker B, Choi JW, Lin ME, Gardell SE, Rivera RR, Kennedy G, et al. Lysophosphatidic acid (LPA) and its receptor, LPA1, influence embryonic schwann cell migration, myelination, and cell-to-axon segregation. *Glia.* (2013) 61:2009–22. doi: 10.1002/glia.22572
  71. Nadra K, de Preux Charles AS, Medard JJ, Hendriks WT, Han GS, Gres S, et al. Phosphatidic acid mediates demyelination in *Lpin1* mutant mice. *Genes Dev.* (2008) 22:1647–61. doi: 10.1101/gad.1638008
  72. Ouro A, Arana L, Rivera IG, Ordonez M, Gomez-Larrauri A, Presa N, et al. Phosphatidic acid inhibits ceramide 1-phosphate-stimulated macrophage migration. *Biochem Pharmacol.* (2014) 92:642–50. doi: 10.1016/j.bcp.2014.10.005
  73. Goebbels S, Oltrogge JH, Kemper R, Heilmann I, Bormuth I, Wolfer S, et al. Elevated phosphatidylinositol 3,4,5-trisphosphate in glia triggers cell-autonomous membrane wrapping and myelination. *J Neurosci.* (2010) 30:8953–64. doi: 10.1523/JNEUROSCI.0219-10.2010
  74. Manna P, Jain SK. Hydrogen sulfide and L-cysteine increase phosphatidylinositol 3,4,5-trisphosphate (PIP3) and glucose utilization by inhibiting phosphatase and tensin homolog (PTEN) protein and activating phosphoinositide 3-kinase (PI3K)/serine/threonine protein kinase (AKT)/protein kinase C $\zeta$ /lambda (PKC $\zeta$ /lambda) in 3T3L1 adipocytes. *J Biol Chem.* (2011) 286:39848–59. doi: 10.1074/jbc.M111.270884
  75. Garofalo K, Penno A, Schmidt BP, Lee HJ, Frosch BP, von Eckardstein A, et al. Oral L-serine supplementation reduces production of neurotoxic deoxy sphingolipids in mice and humans with hereditary sensory autonomic neuropathy type 1. *J Clin Invest.* (2011) 121:4735–45. doi: 10.1172/JCI57549
  76. Skripuletz T, Manzel A, Gropengiesser K, Schafer N, Gudi V, Singh V, et al. Pivotal role of choline metabolites in remyelination. *Brain.* (2015) 138(Pt 2):398–413. doi: 10.1093/brain/awu358
  77. Mak LH, Vilar R, Woscholski R. Characterisation of the PTEN inhibitor VO-OHpic. *J Chem Biol.* (2010) 3:157–63. doi: 10.1007/s12154-010-0041-7
  78. Teres S, Llado V, Higuera M, Barcelo-Coblijn G, Martin ML, Noguera-Salva MA, et al. 2-Hydroxyoleate, a nontoxic membrane binding anticancer drug,

- induces glioma cell differentiation and autophagy. *Proc Natl Acad Sci USA*. (2012) 109:8489–94. doi: 10.1073/pnas.1118349109
79. Kornhuber J, Tripal P, Reichel M, Muhle C, Rhein C, Muehlbacher M, et al. Functional Inhibitors of Acid Sphingomyelinase (FIASMs): a novel pharmacological group of drugs with broad clinical applications. *Cell Physiol Biochem*. (2010) 26:9–20. doi: 10.1159/000315101
  80. Yao JK. Lipid composition of normal and degenerating nerve. In: Dyck PJ, Thomas, PK, Lambert, EH, Bunge RP, editor. *Peripheral Neuropathy, 1984*. 1 ed. Philadelphia, PA: W. B. Saunders Company (1983). p. 510–30.
  81. Hho NVAS. Lipid metabolism in peripheral nerve. In: Dyck PJ, Thomas PK, Lambert EH, Bunge R, editor. *Peripheral Neuropathy, 1984*. 1 ed. Philadelphia, PA: W. B. Saunders Company (1983). p. 531–61.
  82. Goebbels S, Wieser GL, Pieper A, Spitzer S, Weege B, Yan K, et al. A neuronal PI(3,4,5)P3-dependent program of oligodendrocyte precursor recruitment and myelination. *Nat Neurosci*. (2017) 20:10–5. doi: 10.1038/nn.4425
  83. Snaidero N, Mobius W, Czopka T, Hekking LH, Mathisen C, Verkleij D, et al. Myelin membrane wrapping of CNS axons by PI(3,4,5)P3-dependent polarized growth at the inner tongue. *Cell*. (2014) 156:277–90. doi: 10.1016/j.cell.2013.11.044
  84. Cotter L, Ozelik M, Jacob C, Pereira JA, Locher V, Baumann R, et al. Dlg1-PTEN interaction regulates myelin thickness to prevent damaging peripheral nerve overmyelination. *Science*. (2010) 328:1415–8. doi: 10.1126/science.1187735
  85. Figlia G, Norrmen C, Pereira JA, Gerber D, Suter U. Dual function of the PI3K-Akt-mTORC1 axis in myelination of the peripheral nervous system. *Elife*. (2017) 6:e29241. doi: 10.7554/eLife.29241
  86. Hanemann CO, Gabreels-Festen AA, Stoll G, Muller HW. Schwann cell differentiation in Charcot-Marie-Tooth disease type 1A (CMT1A): normal number of myelinating Schwann cells in young CMT1A patients and neural cell adhesion molecule expression in onion bulbs. *Acta Neuropathol*. (1997) 94:310–5.
  87. Robertson AM, Perea J, McGuigan A, King RH, Muddle JR, Gabreels-Festen AA, et al. Comparison of a new pmp22 transgenic mouse line with other mouse models and human patients with CMT1A. *J Anat*. (2002) 200:377–90. doi: 10.1046/j.1469-7580.2002.00039.x
  88. Hu X, Hou H, Bastian C, He W, Qiu S, Ge Y, et al. BACE1 regulates the proliferation and cellular functions of Schwann cells. *Glia*. (2017) 65:712–26. doi: 10.1002/glia.23122
  89. Roberts SA, Lloyd AC. Aspects of cell growth control illustrated by the Schwann cell. *Curr Opin Cell Biol*. (2012) 24:852–7. doi: 10.1016/jceb.2012.10.003
  90. Friede RL. Relation between myelin sheath thickness, internode geometry, and sheath resistance. *Exp Neurol*. (1986) 92:234–47.
  91. Pulido R. PTEN: a yin-yang master regulator protein in health and disease. *Methods*. (2015) 77–78:3–10. doi: 10.1016/j.ymeth.2015.02.009
  92. Hanada K, Nishijima M, Fujita T, Kobayashi S. Specificity of inhibitors of serine palmitoyltransferase (SPT), a key enzyme in sphingolipid biosynthesis, in intact cells. A novel evaluation system using an SPT-defective mammalian cell mutant. *Biochem Pharmacol*. (2000) 59:1211–6. doi: 10.1016/s0006-2952(00)00251-3
  93. Hanada K. Serine palmitoyltransferase, a key enzyme of sphingolipid metabolism. *Biochim Biophys Acta*. (2003) 1632:16–30. doi: 10.1016/s1388-1981(03)00059-3
  94. Pareyson D, Shy ME. Neurofilament light, biomarkers, and Charcot-Marie-Tooth disease. *Neurology*. (2018) 90:257–9. doi: 10.1212/WNL.0000000000004936
  95. Fledrich R, Schlotter-Weigel B, Schnizer TJ, Wichert SP, Stassart RM, Meyer zu Horste G, et al. A rat model of Charcot-Marie-Tooth disease 1A recapitulates disease variability and supplies biomarkers of axonal loss in patients. *Brain*. (2012) 135(Pt 1):72–87. doi: 10.1093/brain/awr322
  96. Soldevilla B, Cuevas-Martin C, Ibanez C, Santacatterina F, Alberti MA, Simo C, et al. Plasma metabolome and skin proteins in Charcot-Marie-Tooth 1A patients. *PLoS ONE*. (2017) 12:e0178376. doi: 10.1371/journal.pone.0178376
  97. Vigo T, Nobbio L, Hummelen PV, Abbruzzese M, Mancardi G, Verpoorten N, et al. Experimental Charcot-Marie-Tooth type 1A: a cDNA microarrays analysis. *Mol Cell Neurosci*. (2005) 28:703–14. doi: 10.1016/j.mcn.2004.11.016
  98. D'Antonio M, Musner N, Scapin C, Ungaro D, Del Carro U, Ron D, et al. Resetting translational homeostasis restores myelination in Charcot-Marie-Tooth disease type 1B mice. *J Exp Med*. (2013) 210:821–38. doi: 10.1084/jem.20122005
  99. Penno A, Reilly MM, Houlden H, Laura M, Rentsch K, Niederkofler V, et al. Hereditary sensory neuropathy type 1 is caused by the accumulation of two neurotoxic sphingolipids. *J Biol Chem*. (2010) 285:11178–87. doi: 10.1074/jbc.M109.092973
  100. Othman A, Bianchi R, Alecu I, Wei Y, Porretta-Serapiglia C, Lombardi R, et al. Lowering plasma 1-deoxysphingolipids improves neuropathy in diabetic rats. *Diabetes*. (2015) 64:1035–45. doi: 10.2337/db14-1325
  101. Schwartz NU, Linzer RW, Truman JP, Gurevich M, Hannun YA, Senkal CE, et al. Decreased ceramide underlies mitochondrial dysfunction in Charcot-Marie-Tooth 2F. *FASEB J*. (2018) 32:1716–28. doi: 10.1096/fj.201701067R

**Conflict of Interest:** The authors declare that the research was conducted in the absence of any commercial or financial relationships that could be construed as a potential conflict of interest.

Copyright © 2020 Visigalli, Capodivento, Basit, Fernández, Hamid, Pencová, Gemelli, Marubbi, Pastorino, Luoma, Riekel, Kirschner, Schenone, Fernández, Armirotti and Nobbio. This is an open-access article distributed under the terms of the Creative Commons Attribution License (CC BY). The use, distribution or reproduction in other forums is permitted, provided the original author(s) and the copyright owner(s) are credited and that the original publication in this journal is cited, in accordance with accepted academic practice. No use, distribution or reproduction is permitted which does not comply with these terms.